ResearchGate

See discussions, stats, and author profiles for this publication at: https://www.researchgate.net/publication/329506220

Determining the spatial profiles of electron and hole concentration, radiative and non-radiative recombination rate near a dislocation defect by combining Raman and photoluminescen...

Conference Paper · June 2018

DOI: 10.1109/PVSC.2018.8548105

CITATIONS
0

READS
23

7 authors, including:

Changkui Hu
Wuhan University of Technology

12 PUBLICATIONS **25** CITATIONS

SEE PROFILE

Fengxiang Chen
Wuhan University of Technology

5 PUBLICATIONS **13** CITATIONS

SEE PROFILE

Timothy H. Gfroerer
Davidson College

47 PUBLICATIONS **346** CITATIONS

SEE PROFILE

M. W. Wanlass
Wanlass Consulting

185 PUBLICATIONS **2,387** CITATIONS

SEE PROFILE

Some of the authors of this publication are also working on these related projects:

III-V semiconductors View project

Defects and Impurities in Semiconductors View project

All content following this page was uploaded by Yong Zhang on 12 December 2018.

The user has requested enhancement of the downloaded file.

Determining the spatial profiles of electron and hole concentration, radiative and non-radiative recombination rate near a dislocation defect by combining Raman and photoluminescence imaging

Changkui Hu,[1,2] Qiong Chen,[1] Fengxiang Chen,[1,2] Heng Lv,[2] T.H. Gfroerer,[3] M.W. Wanlass[4] and Yong Zhang[1,+]

[1]University of North Carolina at Charlotte, Charlotte, NC 28223, USA
[2]Wuhan University of Technology, Wuhan, Hubei 430070, China.
[3]Davidson College, Davidson, NC 28035, USA
[4]National Renewable Energy Laboratory, Golden, CO 80401, USA

[+]Author for correspondence: yong.zhang@uncc.edu

Abstract — **For commonly utilized photoluminescence (PL) imaging, the spatial resolution is dictated by the carrier diffusion length rather than by that dictated by the optical system, such as diffraction limit. Here, we show that Raman imaging of the LO phonon-plasmon (LOPP) coupled mode can be used to recover the intrinsic spatial resolution of the optical system, as demonstrated by Raman imaging of defects in GaAs, achieving a 10-fold improvement in resolution. Furthermore, by combining Raman and PL imaging, we can independently determine the spatial profiles of the electron and hole density, radiative and nonradiative recombination rate near a dislocation defect, which has not been possible using other techniques.**

I. INTRODUCTION

Structural defects often induce adverse effects in semiconductor devices, and impede them from reaching the full performance potential. It is relatively easy to saturate point defect (PD) states in a high quality material under a moderately high carrier injection level, but an extended defect (ED) tends to introduce a very high density of defect states that is practically impossible to be saturated by simply increasing the carrier injection level [1]. Since individual defects vary significantly in their behavior and impact, it is therefore important to locate and investigate them individually and ultimately to identify their atomistic structures. PL imaging is a useful and nondestructive technique for the characterization of individual defects. Without carrier diffusion, the spatial resolution is typically dictated by the point spread function of the optical system. However, when the carrier diffusion length (DL) is greater than the optical limit, the spatial resolution is drastically degraded relative to the capability of the optical system. In the PL image, the defect may visually appear much larger because carriers are depleted in the surrounding region over a distance comparable to DL from the defect site [1-3]. In addition, Raman imaging has long been used to characterize mesoscopic or macroscopic structural inhomogeneity in semiconductors. However, because Raman efficiencies are typically many orders lower than PL, and defect-induced perturbations to vibrational properties tend to be very local, it is impractical in most realistic situations to probe individual microscopic defects with conventional Raman spectroscopy. Therefore, for a high quality sample, i.e., with a long DL, a new technique is required to better resolve non-radiative defects in the presence of diffusing carriers. Furthermore, commonly known CW and time-resolved characterization techniques are not possible to determine independently the electron and hole carrier density, radiative and nonradiative recombination rate near a defect. In the present work [4], we address two issues: (1) how can we achieve beyond diffusion limit (BDL) defect imaging in semiconductor using the LOPP Raman scattering technique? and (2) how can the spatial dependence of the electron density, hole density, radiative recombination rate, and non-radiative recombination rate near a dislocation-like defect be determined separately?

II. PRINCIPLE

The coupling of the LO phonon with free electrons (plasmon) from doping leads to the formation of hybrid modes L_+ and L_-, and the Raman signal of L_+ is very sensitive to the carrier density in both frequency and intensity [4]. The same effect is observed with photo-generated electron-hole plasmas [5]. The underlying physics for the drastically improved spatial resolution lies in (1) the Raman frequency is a superlinear function of carrier density n; (2) the Raman cross-section R(n) decreases with increasing n; and most importantly (3) a Gaussian or Lorentzian type lineshape function offers a very strong dependence of the Raman intensity on the frequency shift. The combination of these properties results in that the Raman signal of the L_+ mode exhibits a much stronger dependence on n, and thus a much more rapid spatial variation than that of PL.

Because LOPP Raman imaging provides a straightforward method to obtain the spatial variation n(r) near the defect,

combining with PL mapping, we can obtain the impact of the defect to the radiative recombination rate $W_r(r)$ through $I_{PL}(r) = n(r)Wr(r)$ near the defect, which is otherwise not normally accessible (e.g., PL decay time would only give the total decay rate). Writing $W_r = \gamma\ p$ with p being the hole concentration and γ the recombination coefficient (a constant), $W_r(x)$ reflects the hole distribution with diffusion. So we can plot the absolute hole density by assuming away from the defect under high excitation density, n = p. Additionally, we can further infer information about the nonradiative recombination rate $W_{nr}(r)$ near the defect. Because under a local excitation/local detection (L/L) mode the carrier diffusion away from the excitation site represents an additional loss mechanism, we write the total loss as $W_{loss} = W_{nr} + W_d$ with W_{nr} being the genuine nonradiative recombination loss associated with both uniformly distributed point defects and the particular dislocation, and W_d being an effective rate for the diffusion loss at the excitation site. From the rate equation, we may have $W_{loss} = G[1-\eta_{PL}I_{PL}(r)/I_{PL}(\infty)]/n(r)$, where G is the generation rate, $I_{PL}(r)$ and n(r) are the PL intensity and electron density at a distance r from the defect, and η_{PL} is the PL efficiency far away from the defect ($\eta_{PL} \leq 1$ due to nonradiative loss through point defects and diffusion).

III. Experiment

A. Materials and method

Two GaInP/GaAs/GaInP double heterostructures were used to examine the general applicability of the approach for different conditions. Sample 1 (S1) has a 2 µm GaAs layer sandwiched between two 50 nm GaInP layers, all nominally undoped with a n-type background doping level of ~5×10^{14} cm^{-3}. Sample 2 (S2) also has a 2 µm GaAs active layer, but with 100 nm GaInP barriers. The upper half of the top barrier is doped in n-type to ~$5\ \times10^{18}$ cm^{-3}, and the lower half is un-doped. The samples are all grown on a GaAs substrate with a GaAs buffer layer via metal-organic vapor phase epitaxy. These samples have very low dislocation-type defect densities.

All experiments were conducted at room temperature using a Horiba LabRAM HR800 confocal Raman microscope using a 100× microscope objective lens (NA=0.9) and a 532nm laser, yielding a diffraction-limited excitation spot size of about 720 nm in diameter. The PL and Raman signals were acquired via a CCD detector with laser powers varying from 20 to 200 µW at the sample. The PL and Raman images were acquired in raster scan mode.

B. Result and discussion

Fig. 1 contrasts PL and Raman imaging results near an isolated defect in each of the two samples. The PL images use the signal at 870 nm (20 nm bandwidth), and the Raman images use the LO mode (0.5 cm^{-1} band width) of the defect site. For S1, the DL derived from the PL image of Fig. 1(a) is ~25.7 µm (using the method of Ref. [3]). Already because of using raster scan (L/L mode), the effective defect impact range is already significantly smaller than the DL [3]. However, the effective defect range in the Raman image Fig. 1(c) is further reduced to just over 1 µm, as predicted above. Fig. 1(e)

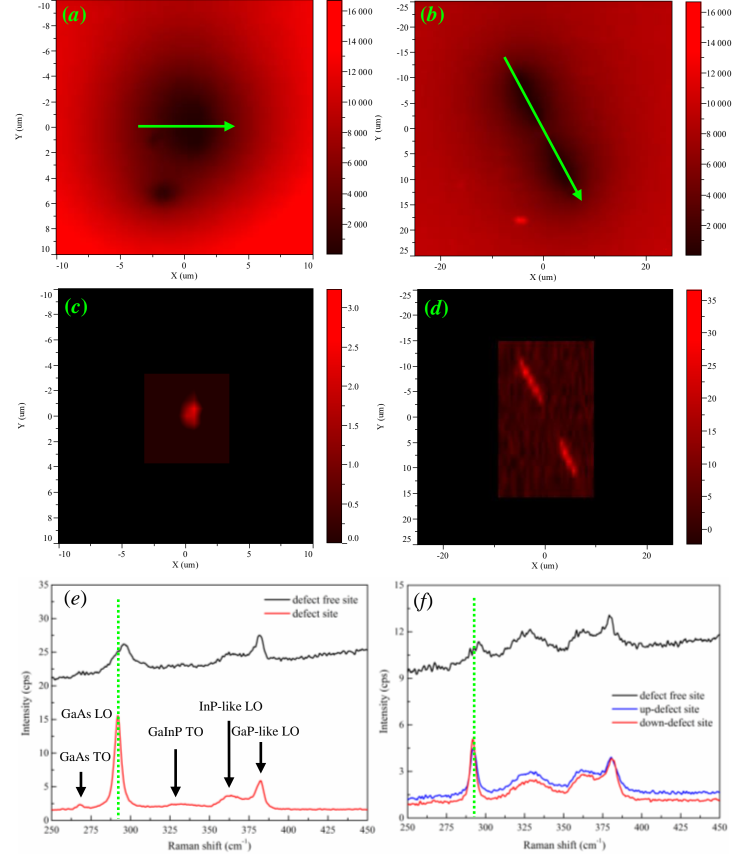

Fig. 1. PL and Raman images near a defect and the typical Raman spectra at and away from the defect for two GaAs samples. (a) and (b): PL images, (c) and (d): Raman images, (e) and (f): Raman spectra (data was not obtained in the black outer region). Left column – S1 (at 3.7×10^4 W/cm^2), right column – S2 (at 5.6×104 W/cm^2).

compares Raman spectra at the defect and defect-free site, where the GaAs LO or L_+ mode is significantly blue-shifted, broadened and weakened at the defect-free site, which explains the superior spatial resolution in Raman imaging. For S2, a pair of close by defects is examined. In PL imaging, with DL ≈ 24.2 µm, they are resolvable under L/L mode although the diffusion effect remains significant as in Fig. 1(b). However, with Raman imaging, Fig. 1(d), the spatial resolution is virtually not affected by the diffusion. The Raman spectra in Fig. 1(f) exhibit the similar contrast between the defect and defect-free site as in S1. Clearly, Raman mapping is a generally applicable and effective tool to achieve BDL defect imaging.

Fig. 2 shows the evolution of the Raman spectrum using a line scan across the center of the defect in S1, as illustrated in

Fig. 1(a). It reveals the drastic changes of the L_+ mode near the defect.

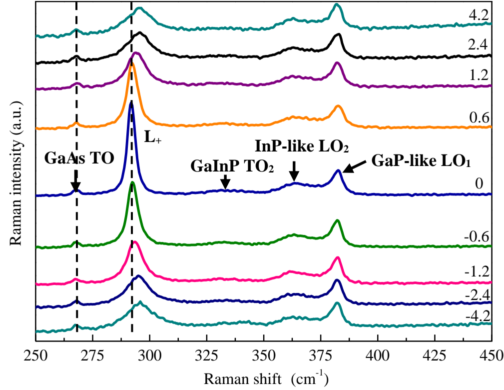

Fig. 2. Raman spectra at different displacements from the defect

Fig. 3 examines the spatial dependence, for the electron density, hole density, Raman intensity at ν_{LO}, PL intensity at the bandgap energy, radiative and nonradiative recombination rates.

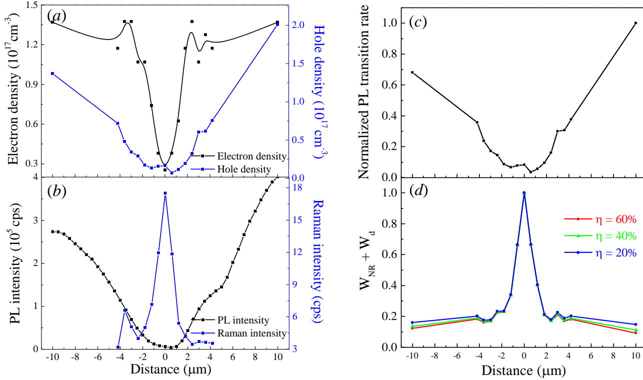

Fig. 3. Raman and PL properties near the defect in S1. (a) Spatial profiles of the electron density and hole density. (b) Spatial profiles of Raman intensity at ν_{LO} and PL intensity at the bandgap energy. (c) Normalized radiative recombination rate. (d) Normalized nonradiative recombination loss rate.

Fig. 3(a) shows that the depletion of the electrons is highly localized near the defect, recovering to the background level within about 2 μm, whereas the variation of the hole density is much gradual. Despite in general the electron DL is much longer than hole DL, the electron density is not affected by the defect as soon as moving away from the defect. This finding suggests that the defect is a hole trap. Fig. 3(b) contrasts the spatial variation of the L_+ mode intensity and the PL peak intensity. The PL intensity reaches the background value within about 10 μm, which is roughly half of the DL, in the L/L mode, but the Raman intensity reaches the background level within about 2 μm, about 1/10 of the DL. Given the fact that beam size is about 0.7 μm, the rapid Raman intensity change is the dominant effect offering the high spatial resolution in the Raman image. Fig. 3(c) plots the (normalized) PL transition rate $W_r(x)$, which essentially reflects the hole density distribution. This result reveals very important information about the defect that is not readily available in PL mapping alone. The mismatch in the electron and hole distribution implies the formation of a polarization field near the defect. Therefore, the carrier diffusion process could be much more complicated than we thought [3]. Fig. 3(d) shows that the total loss W_{loss} is very high in a small region near the defect, similar to the electron distribution in Fig. 3(a), but quickly drops off beyond that to a background level that is only weakly depending on the choice of η_{PL}, where W_d likely dominates, which is consistent to the finding that carrier diffusion affects carrier lifetime [7].

IV. Conclusions

Utilizing the nonlinear dependence of the LO phonon – plasmon coupled Raman mode in Raman imaging, a close to diffraction limit spatial resolution has been achieved in semiconductor defect imaging where the carrier diffusion length is up to 20 times larger. We anticipate that the spatial resolution can be even better if sub-diffraction limit optical excitation is used. This approach offers superior spatial resolution relative to the more commonly adopted PL imaging. Furthermore, by combining Raman imaging with PL imaging, we can obtain several elusive physical parameters, including electron and hole densities and radiative and nonradiative recombination rates in the vicinity of an individual dislocation-like defect.

Acknowledgement

The work at UNCC was supported by ARO/MURI (W911NF-10-1-0524) and ARO/Electronics (W911NF-16-1-0263), at WUT by Project supported by the National Natural Science Foundation of China (Grant No.51702245). CKH acknowledges the support from China Scholarship Council for his visit at UNCC, YZ acknowledge the support of Bissell Distinguished Professorship at UNCC.

References

[1] T. H. Gfroerer, Y. Zhang and M. W. Wanlass, "An extended defect as a sensor for free carrier diffusion in a semiconductor," *Applied Physics Letters*,vol.102, pp.012114, 2013.

[2] C. Donolato, "Modeling the effect of dislocations on the minority carrier diffusion length of a semiconductor," *Journal of Applied Physics*, vol.84, pp. 2656-2664, 1998.

[3] F. Chen, Y. Zhang, T. H. Gfroerer, A. N. Finger and M. W. Wanlass, "Spatial resolution versus data acquisition efficiency in mapping an inhomogeneous system with species diffusion," *Sci. Rep.*, vol.5, pp.10542, 2015.

[4] C. Hu, Q. Chen, F. Chen, T.H. Gfroerer, M.W. Wanlass and Y. Zhang, "Overcoming diffusion-related limitations in semiconductor defect imaging with phonon-plasmon coupled

mode Raman scattering", Light: Sci. & Appl. doi: 10.1038/s41377-018-0016-y.
[5] A. Mooradian and G. B. Wright, "Observation of the Interaction of Plasmons with Longitudinal Optical Phonons in GaAs," *Physical Review Letters*, vol.16, pp.999-1001, 1966.
[6] A. Pinczuk, J. Shah and P. A.Wolff, "Collective Modes of Photoexcited Electron-Hole Plasmas in GaAs," *Physical Review Letters*, vol. 47, pp.1487-1490, 1981.
[7] D. Kuciauskas, S. Farrell, P. Dippo, J. Moseley, H. Moutinho et al., "Charge-carrier transport and recombination in heteroepitaxial CdTe," J Appl Phys. 116, 123108, 2014.

View publication stats